Chapter 5

L1$_0$-FePt granular films for heat assisted magnetic recording media

Kazuhiro Hono and Yukiko K. Takahashi
Magnetic Materials Unit, National Institute for Materials Science
1-2-1 Tsukuba, 305-0047, Japan
kazuhiro.hono@nims.go.jp

FePt-C nanogranular films are coming close to the actual application as recording media for the next generation high density recording system, heat assisted magnetic recording (HAMR). To optimize the L1$_0$-FePt nanogranular structure suitable for high areal density recording, various combination of segregants and seed layer materials have been explored. In this chapter, we review recent investigations aiming at achieving the ideal nanogranular structure for HAMR media.

1.1 INTRODUCTION

Hard disk drives (HDD) have been a major storage device in computers for the last 50 years and more recently in home video recording systems and cloud computing due to their large storage capacity, low bit cost and non-volatility. Although solid state devices (SSD) are now replacing the storage devices for notebook computers, HDDs will continue to be a major player in the data storage industry. The number of HDDs sold in 2012 was approximately 800 million, nearly one tenth of the world population! To meet the demand for rapidly increasing digital data and to keep the competitiveness of HDD with other emerging storage devices, the areal density of the HDDs must keep increasing.

The areal density of the current HDD is approximately 800 Gbit/in^2. In the past, it had shown an increase of 100% every year, but the recent growth rate has slowed down to 30%, reaching saturation [1]. Although various technological improvements have been made in both heads and media in the current perpendicular recording (PMR) system, ~1 Tbit/in^2 is considered to be the limit for the PMR method. Due to the recent improvements in signal processing using shingled magnetic recording, the areal density of PMR is expected to increase marginally above 1 Tbit/in^2. However, a transition to a new magnetic recording method must be realized in the near future to sustain the growth of the recording industry.

Heat assisted magnetic recording (HAMR) is a technology close to commercialization. However, a new medium that is totally different from the current one must be developed using a high magnetocrystalline anisotropy ferromagnetic material. The current PMR recording media are CoCrPt-SiO$_2$ nanogranular films, in which nanosized CoCrPt columnar grains with the hcp structure are dispersed uniformly with a strong [0001] fiber texture as shown in **Fig. 1**. Such films are deposited on glass substrates with an amorphous CoTaZr soft magnetic underlayer and the

Ru seed layer that optimizes the grain size and the crystallographic orientation of the CoCrPt grains. Since the easy axis of magnetization of the CoCrPt alloy is [0001], this crystallographic texture gives rise to a strong perpendicular magnetic anisotropy (PMA). Each grain of approximately 8 nm in diameter is magnetically isolated and one bit contains multiple CoCrPt grains that are magnetized in the same direction as shown in **Fig. 2**. The bit size for the areal density of 1 Tbit/in^2 will be ~25 × 25 nm^2, in which more than 10 ferromagnetic grains must be contained to attain a sufficiently high signal to noise ratio. This suggests that the ferromagnetic grains must be refined further to ~4 nm for an areal density above 1 Tbit/in^2. This requirement makes the ferromagnetic grains thermally unstable as the magnetocrystalline energy K_uV becomes comparable to the thermal energy k_BT, where K_u is the uniaxial magnetocrystalline constant, V is the volume of the grain, k_B is the Boltzmann constant. In order to keep the recorded information for longer than 10 years, K_uV/k_BT must be larger than 60. This means that the ferromagnetic material with high magnetocrystalline anisotropy such as $L1_0$-FePt, $L1_0$-CoPt, $Nd_2Fe_{14}B$, and $SmCo_5$ must be used for high density recording, where V becomes as small as ~4 × 10^{-26} m^3 [2, 3]. As the media require long-term endurance, the rare earth compounds are unlikely to be selected as they are very susceptible to oxidation and corrosion. As a result, $L1_0$-FePt phase is currently considered to be the most promising material for HAMR media.

While K_u of the CoCrPt alloy is ~0.3 MJ/m^3, the $L1_0$-ordered FePt has an order of magnitude larger magnetocrystalline anisotropy of 6.6 MJ/m^3, which makes the minimum size of stable ferromagnetic grains ~ 4 nm for spheres and 2.4 nm for cylinders [4]. In addition, the magnetic polarization of the $L1_0$-FePt phase is μ_0M_s~1.4 T, which is large enough to gain sufficient signal to noise ratio with the film thickness of less than 8 nm. However, if hard magnetic grains become so small, the magnetic field required to switch the magnetization of the grain (H_N) or coercivity (H_c) will increase enormously. The typical switching field or μ_0H_c for the current recording media is about 0.8 T, while that of the nanosized $L1_0$-ordered FePt will be higher than 3 T. The highest magnetic field that can be generated using a write head is limited to about 1.5 T using the soft ferromagnet with the highest saturation magnetic flux density of 2.35 T for $Fe_{65}Co_{35}$ [5]. Since the reduction of grains of hard magnetic materials to a nanosized dimension leads to substantial increase of coercivity larger than 1.5 T, these grains will not be writable with the head field. This is known as "trilemma" of magnetic recording. Ultrahigh density magnetic recording requires nanosized ferromagnetic grains, which become thermally unstable below certain sizes. To overcome this problem, a high K_u material must be used; then the switching field of the grains becomes too large to write.

To overcome the trilemma problem, the magnetization switching must be assisted by some external energy such as heat or microwave. HAMR technology uses heat to assist the magnetization switching of high K_u grains using a well-focused laser beam [6, 7]. As temperature increases, the coercivity of the grains decreases because of reduced anisotropy field. Writing is done at the temperature slightly lower than Curie temperature, where the coercive field becomes smaller than the head field of about 1 T. When temperature decreases rapidly after writing, the high K_u nanosized grain has sufficient thermal stability for permanent recording. To realize HAMR, new technologies are required in both the write head and the medium. The HAMR head has been demonstrated recently using a plasmonic antenna [6]. The tolerance of near field optical transducers is the most critical issue for improving the reliability of HAMR HDD to a practical level. As to the media, the FePt-C system is the only viable system for HAMR media at this moment. However, the grain size and in-plane magnetic component are not reduced to the desired level yet. Although the first HAMR HDD is anticipated to use the FePt-C based media with a recording density slightly higher than the upper limit of PMR, further increase in the areal density towards 4 Tbit/in^2 depends on how we can optimize the nanogranular structure of the

FePt-C based media on glass disks through various buffer layers for heat sinking and crystal orientation alignments. In this paper, we review the history of the development and optimization of the $L1_0$-FePt based nanogranular films based on published literature.[*]

1.2 IDEAL STRUCTURE FOR HAMR MEDIA

The desirable HAMR media should be comprised of densely dispersed ferromagnetic grains exhibiting high magnetocrystalline anisotropy of larger than 5 MJ/m^3 with a uniform grain size of ~4 nm with a center to center distance of 5 nm. The size distribution of the grains must be lower than 10% for attaining sufficiently low switching field distribution (SFD). For sufficient signal to noise ratio, the grain shape should be columnar with the grain aspect ratio h/D>1.5, where h is the height and D is the diameter of FePt grains. Such an ideal film structure is schematically shown in **Fig. 2** [8] and the proposed HAMR media requirements for 2 and 4 Tbit/in^2 released from the Advanced Storage Technology Consortium (ASTC) is shown in **Table 1** [9]. The film must exhibit high coercivity above 3 T, more than 4 times larger than that of the current recording media. In addition, the microstructure should be realized on commercially viable substrates such as glass. The key factors to control the microstructure of HAMR media are (i) ordering the A1-FePt phase to the $L1_0$ structure by annealing without grain coarsening, (ii) obtaining strong perpendicular magnetic anisotropy (PMA) with low in-plane component, (iii) attaining nanometer diameter (ideally 4 nm) with a narrow size distribution of less than 10%, (iv) low surface roughness (R_a<0.4 nm) because of narrow head-media distance for high density recording. Fulfilling all of the above requirements has been challenging, and many investigations on the optimization of FePt-based nanogranular structure have been made since 2000. Seagate has recently demonstrated HAMR over the areal density of 1 Tbit/in^2 using supposedly FePt based granular media [10]. However, further microstructure optimization is essential to extend the areal density to 4 Tbit/in^2.

1.2.1 *A1→L1₀ ordering*

Although the $L1_0$-FePt phase is thermally stable below 1300°C, the FePt films sputter-deposited below 400 °C have the disordered A1 structure because of a kinetic constraint. Since the melting temperature of equiatomic FePt alloy is about 1830 K, the volume diffusion is very sluggish below 917 K (~640 °C). This means that the sputtered A1 film has to be annealed above 640 °C to make them transform to the $L1_0$ structure by volume diffusion [11] or must be deposited on heated substrates [12]. Hence, lowering the kinetic ordering temperature from the A1 to $L1_0$ structure was considered to be essential, and the effect of various alloying elements to enhance the kinetics of $L1_0$ ordering was investigated. Among various elements, Cu and Ag were reported to be effective to reduce the kinetic ordering temperatures in continuous polycrystalline films [12-14]. By alloying FePt with Cu, the ordering temperature decreases to 400 °C while binary A1 FePt does not order below 600 °C [12]. The Cu alloying, however, leads to the reduction of the magnetocrystalline anisotropy energy [15]. Note that most of these investigations on the effect of additives on ordering were carried out on continuous polycrystalline films, in which ordering was accompanied by recrystallization of nanocrystalline films [16]. So the elements that are effective in reducing the ordering temperature of continuous films do not necessarily work on

---

[*] Many investigations carried out in industry are kept confidential. It is beyond the authors' knowledge to make comprehensive review including the efforts carried out in industrial laboratories. Hence, the review is based on published literatures only.

the FePt-X granular films, where FePt grains are isolated by segregants [17]. It should be also noted that there is a size dependence of $L1_0$ ordering when the grain size becomes smaller than 4 nm [18-20]. This is because the surface energy become dominant compared to the volume free energy, where A1 phase become more stable than the $L1_0$ phase. This size dependence of order may become significant when the grain size is successfully reduced to less than 4 nm for 4 Tbit/in² areal density in the future.

1.2.2 *[001] texture*

To apply the $L1_0$-ordered FePt thin film to HAMR media, the magnetic easy axis must be aligned normal to the film plane. However, the FePt thin films deposited onto amorphous substrates tend to develop a [111] texture because the (111) plane of A1 phase has the lowest surface energy. In early studies of FePt thin films, (001) oriented MgO single crystalline substrates were used to grow PMA films [21-27]. MgO has the NaCl structure with the lattice parameter of 0.421 nm, while the lattice parameters of $L1_0$-FePt are a=0.386 nm and c=0.373 nm in the fct lattice or a=0.273 nm and c=0.373 nm in the bct lattice. The (001) FePt grows on (001) MgO with the cube-to-cube orientation relationship with the lattice mismatch of about 8.3%. Because of this large misfit, the FePt is subject to receive expansion stress to the a- and b-axis directions, thereby growing only one variant for A1→$L1_0$ ordering on heated MgO substrate. This gives rise to the strong PMA to the $L1_0$-ordered FePt thin films.

Based on detailed TEM observations, Shima *et al.* showed the $L1_0$-ordered FePt film grows with the Volmer-Weber (VW) mode on the (001) single crystalline MgO at 700 °C [26]. The coercivity of these films was as high as 4 T, which decreases abruptly when the isolated grains are percolated for nominal film thickness of larger than 40 nm. The growth mode changes from the VW mode to the Frank-Van der Merwe (FV) mode when the substrate temperature is decreased below 350 °C [26] as shown in **Fig. 3**. This nature of the Volmer-Weber growth on the MgO substrate is essential for the formation of well-isolated FePt grains in recording media. The degree of order increases above 450 °C, about 200 °C lower than $T_m/2$, where T_m is the melting temperature of FePt. This is because the $L1_0$ ordering progresses *in-situ* on heated substrate by surface diffusion. The coercivity of the films depends on both the morphology of the FePt grains and the degree of $L1_0$ order. Even if the degree of $L1_0$ order is high, H_c can be low if the FePt becomes continuous, as the magnetization switching can occur by the domain wall motion without any pinning after a nucleation. Single domain grains of about 50 nm show very large coercivity of 7 T at room temperature, which is nearly 50% of the anisotropy field H_A [28]. This level of coercivity with respect to the anisotropy field has never been observed in other hard magnetic systems.

One may wonder if the large mismatch between MgO and FePt may influences the intrinsic magnetic properties of the $L1_0$-oredered FePt films such as magnetization, M_s and K_u. Hotta *et al.* investigated the thickness dependence of the magnetic properties of FePt films deposited on heated MgO, $MgAl_2O_4$, and $SrTiO_3$ (001) single crystalline substrates that induce the lattice mismatches of ~9, 5, and 1 %, respectively [29]. Based on the results, they concluded that the magnitude of the lattice mismatch does not give any influence on M_s, K_u and the long range order parameter, S. On the other hand, Ding *et al.* investigated the K_u of the FePt film sputter-deposited on MgO(001) substrates through various buffer layers, such as Pt, Cr, CrMo, and concluded that the critical lattice mismatch around 6% is the most suitable for improving the $L1_0$ ordering of FePt [30]. However, the results need to be carefully interpreted because of the possibility of interdiffusion of Cr into the FePt layer.

In recording applications, single crystalline substrates cannot be used because of their high cost. While FePt thin films were prepared on heated single crystalline (001) MgO substrate in early fundamental studies, practical seed layer must be deposited on either glass or amorphous substrates. Jeon et $al.$ reported the growth of PMA FePt polycrystalline films on the (001) textured MgO seed layer that was deposited on a thermally oxidized Si substrate [31]. Thereafter, Xu et $al.$ reported the successful growth of (001) textured FePt polycrystalline films (t=50 nm) on $Cr_{91}Ru_9$ substrate with PMA [32]. However, since the Cr diffuse into FePt at elevated substrate temperature, the growth temperature was limited to 400 °C. Hence, only a low perpendicular coercivity of ~0.4 T was reported. Although the (110) Cr plane is the most close-packed plane, a [001] texture develops in a Cr buffer layer at an optimized condition, which led to the [001] texture of FePt on CrRu. The lattice mismatch of 5.8 % with the FePt (001) causes the expansion of the in-plane FePt (100) lattice. Since the c/a ratio of $L1_0$ FePt phase is 0.964, the slightly higher lattice mismatch between Cr (110) and FePt (100) assist the transformation from the A1 phase to the $L1_0$ phase. By adding Ru into Cr thin films, the lattice mismatch can be tuned as the atomic radius of Ru is larger than that of Cr. Xu et $al.$ showed that 10 at.% Ru optimized the lattice mismatch for $L1_0$ ordering [32]. With in-$situ$ annealing, perpendicular FePt [001] texture with good $L1_0$ order was obtained at a relatively lower temperature of 350°C, whereas a temperature over 600 °C was required to achieve high $L1_0$ order by post-deposition annealing. This means that a reduction of the ordering temperature by 200 °C was achieved by the in-$situ$ annealing using the CrRu underlayer. Although Cr based underlayer reduces the ordering temperature, Cr diffusion into FePt deteriorates the magnetocrystalline anisotropy. Chen et $al.$ inserted a thin MgO layer as a diffusion barrier of Cr and reported the growth of (001) textured $L1_0$-FePt polycrystalline films with strong PMA on glass substrates [33]. In their film stack, the orientation relationships of FePt(001)[100] // MgO(001)[100] // CrRu(200)[110] were confirmed. The coercivity was enhanced to 1.2 T in this film stack.

Later, Perumal et $al.$ reported [001]-textured FePt particulate films grown on [001] textured MgO seed layer that was pre-deposited on thermally oxidized Si [34]. This work has shown that the intermediate layer such as CrRu is not essential to control the texture and the microstructure of FePt films. However, there is one drawback in the MgO seed layer. Since it is insulator, the MgO seed layer must be grown using RF sputtering, which causes slow sputtering rates and some undesired grains. Ideally, the seed layer could be sputtered with a DC power, so electrically conductive materials are more desirable as a seed layer. Varaprasad et $al.$ reported [001] textured FePt film grows on a $(Mg_{0.2}Ti_{0.8})O$ seed layer. $(Mg_{1-x}Ti_x)O$ is electrical conductive having the NaCl structure for a wide range of x [35]. This seed layer shows strong [001] texture on amorphous substrates and can induce the growth of [001] FePt ferromagnetic layer. However, the surface energy appears to be lower than that of MgO(001). Hence, the wettability of FePt on MTO is good, hindering the particulate growth of FePt layers using the FePt-C system. $(Mg_{1-x}Ti_x)O$ (MTO) has the identical rock salt structure for a wide range of x, i.e., $0<x<0.8$, and the surface energy of Mg-rich MTO become close to that of MgO. So MTO has a potential to be a seed layer to replace MgO, if the nanogranular structure of the FePt layer can be optimized.

1.2.3 FePt-C granular films

In order to use thin films as a recording medium, exchange decoupled nanosized ferromagnetic grains must be densely dispersed in two dimensions. Early investigations on FePt thin films were mainly done to obtain high coercivity in magnetically coupled polycrystalline films [10, 12-14], in which ordering occurs accompanied by recrystallization [13], but the ordering process in completely isolated grains must progress continuously without grain boundary

migration [17]. One of the earliest works on the FePt-Al-O granular film by Watanabe *et al*. [36,37] reported randomly oriented grains of about 5 nm in diameter in the as-sputtered condition. In this work, FePt was co-sputtered with aluminum and oxygen on a thermally oxidized Si substrate at room temperature. As a result, the structure of the FePt grains in the as-sputtered condition was A1 without any crystallographic texture. High-temperature annealing was necessary to order the A1 phase to the $L1_0$ structure, but this caused a coarsening and coalescence of the $L1_0$ -FePt grains. Luo *et al*. [38] reported perpendicular anisotropy films fabricated by annealing FePt/B_2O_3 multilayers deposited on glass substrates. However, the microstructure reported in the work is far from the ideal microstructure that can be used as a recording medium. Peng also investigated the multilayer deposition of [FePt/MgO]$_n$ on a [001] textured MgO seed layer to form FePt-MgO composite films, but the FePt grains were not well isolated and no PMA was observed [39].

In 2003, Ko *et al*. [40] and Perumal *et al*. [41,42] reported the FePt-C granular structure with PMA having an average grain size of 4 nm. They co-sputtered FePt and C on MgO (001) single crystalline substrates at 400 °C. Since C has no solubility with Fe and Pt, C was rejected from FePt nanograins making the FePt grains magnetically isolated through intergranular carbon. The $L1_0$ ordering occurs during the film deposition with a strong [001] texture. Following this work, Chen *et al*. have grown FePt-C films by co-sputtering FePt and C targets on glass substrates through $Cr_{90}Ru_{10}$/Pt buffer layers at 350 °C [43]. They obtained very fine uniform granular structure of about 6 nm grain size with a perpendicular coercivity of about 0.37 T. Because of the usage of the CrRu underlayer, the substrate temperature was limited to 350 °C, which was not sufficient to give high degree of $L1_0$ order. Subsequently, Chen *et al*. [44-47] deposited FePt-C films on glass substrate through a CrRu buffer layer and MgO seed layer and demonstrated [001] textured FePt-C granular film with a higher coercivity of ~1.4 T. From the cross sectional image of the FePt-C magnetic layer, they have shown the formation of second layer in the FePt-C magnetic layer. Also, they reported that columnar grains can be grown by increasing the sputtering rate. However, the in-plane TEM observation showed the FePt grains were interconnected.

In 2008, Perumal *et al*. reported FePt-C based PMA granular films with narrow size distribution of isolated $L1_0$-FePt grains [48]. The average grain size of the $L1_0$-ordered FePt was ~5.5 nm with a 2.3 nm size dispersion. The films were grown by co-sputtering Fe, Pt and C on the MgO seed layer that was pre-deposited on thermally oxidized Si substrate. This is the first media-like structure obtained from FePt based films. The key to the success was to sputter-deposit FePt and C on a heated substrate so that the ordering to the $L1_0$ structure can progress during the film growth at a much lower temperature than that required for the post-deposition annealing (~640 °C). During the growth of the films at elevated temperature, atomic transport occurs by surface diffusion, thereby enhancing the kinetics for $L1_0$ ordering at the substrate temperature. While $L1_0$ ordering progresses during the growth, carbon is rejected from FePt forming a thin channel of amorphous carbon as shown in **Fig. 4**. However, the coercivity was only in the order of 0.8 - 1.5 T due to the low degree of the $L1_0$ order in the FePt grains, and a higher coercivity had to be achieved for the HAMR media.

1.2.4 (FePt)$_{0.9}$Ag$_{0.1}$-C granular films

The excellent FePt-C nanogranular structure demonstrated by Perumal *et al*. convinced the community that FePt-C could be a HAMR medium. However, the coercivity of the film was still too low for the HAMR media requirement [48,49]. In early studies of FePt continuous films, Platt *et al*. showed that the kinetic ordering temperature of FePt can be reduced by the addition of Ag [50]. Following this concept, Zhang *et al*. succeeded in processing a nanograin-dispersed

PMA thin film with a mean grain diameter of 6.1 nm, size dispersion of 1.8 nm, and coercivity of 3.7 T by adding Ag to the FePt-C granular films [51]. To align the [001] crystal orientation perpendicular to the film, a thin layer of MgO was grown on a Si substrate, followed by sputtering a (FePt)Ag-C magnetic layer. The $(FePt)_{0.9}Ag_{0.1}$-40vol.%C film had the highest grade of grain dispersion and the [001] texture of $L1_0$-FePt. The in-plane TEM image in **Fig. 5 (a)** shows the uniform microstructure with an average grain size of 6.1 nm and the size distribution of 1.8 nm. The pitch distance (center to center) was about 9.6 nm. The SAED pattern shows the FePt grains have strong c-axis texture. **Fig. 5** (b) shows the magnetization curves of out-of-plane and in-plane directions. The film has strong PMA. The perpendicular μ_0H_c is about 3.5 T and the anisotropy field estimated by the cross point of the in-plane and out-of-plane curves is about 6.5 T. The estimated K_u of the FePt grains is 4.3×10^6 J/m^3, which is half of that reported for a bulk $L1_0$-FePt. The high K_u and μ_0H_c result from the high degree of $L1_0$ order, 0.9. Because of the high anisotropy FePt grains, the thermal stability (K_uV/k_BT) estimated by the time dependent H_c measurement was about 200, indicating that the stored information in the media is thermally stable for more than 10 years [52]. Subsequent HAMR static tester results demonstrated the areal density of 550 Gbit/in^2 on this medium as shown in **Fig. 5** (c) [53]. This recording density was the highest one achieved by HAMR at that time and was comparable to that of the conventional PMR method.

To understand the mechanism of the enhancement of H_c and the anisotropy of FePt-C granular film by the addition of Ag, a detailed chemical analysis was carried out using aberration corrected scanning transmission electron microscopy (STEM). **Fig. 6** shows STEM-energy dispersive X-ray spectroscopy (EDS) elemental maps of Fe and Ag in the $(FePt)_{0.9}Ag_{0.1}$-28vol%C film. It shows that the FePt grains are enveloped by Ag-rich shells [54]. In addition, X-ray absorption fine structure XAFS measurements revealed that Ag of the shell had a fcc-like structure. Ag was confirmed to be dissolved in FePt grains when the $(FePt)_{0.9}Ag_{0.1}$-C was deposited at room temperature, the formation of the Ag-rich shell can be interpreted as a result of Ag rejection from the FePt grains during the deposition process. The Ag rejection is possible only with the diffusion of Ag through vacancy motion, suggesting that the Ag alloying enhances the diffusion in FePt crystals, thereby enhancing the kinetics of A1 $\rightarrow$ $L1_0$ ordering.

Since the (FePt)Ag-C nanogranular films can be deposited easily by sputtering on the MgO seed layer, where crystal orientations are naturally aligned to the [001] direction during the film growth, the they can be fabricated on substrates other than thermally oxidized Si, including glass substrates and amorphous metals. From this viewpoint, the (FePt)Ag-C system has high potential to be extended to industrially viable production lines. Using a semi-industrial sputtering machine with a triode target, Hitachi Global Storage Technologies (HGST) reported similar microstructure on glass substrates with NiTa amorphous heat sink layer [55,56].

Although the microstructure and magnetic properties attained in the (FePt)Ag-C was so close to that required for practical use, there have been two critical issues to be resolved: one is to obtain a small roughness on the surface and the other is to grow the FePt grains in a columnar shape with an aspect ratio $h/D>1.5$ as shown in **Fig. 2**. These two problems stem from the strong driving force for the phase separation between FePt and C. The reason why the FePt-C system shows well-isolated planar structure is that the FePt and C are entirely immiscible with strong repulsive nature. Hence, while the plan-view show nice grain separation, the cross sectional image show the formation of second layer on the top of the FePt grains that were grown on MgO seed layer epitaxially as shown in **Fig. 4**. Since the second layer has no orientation relationship with the underlayer being separated by amorphous carbon, the perpendicular anisotropy is substantially degraded. This is because the C has too strong driving force for phase separation. Although strong phase separation makes the grain isolation better in the lateral direction, this in turn interrupts the columnar growth in the growth direction and causes another grain to nucleate

on an underlying grain. In order to overcome this issue, various segregants other than C have been explored.

1.2.5 Exploration for a new segregant for FePt-X media

Before the FePt-C system was found to be suitable for achieving the granular structure for a HAMR medium, various FePt-X systems including the FePt-SiO$_x$ system were thoroughly investigated. Seki et al. reported the formation of fine FePt-SiO$_2$ granular structure [57]. However, the coercivity becomes very low when the substrate temperature was decreased to achieve the grain size of less than 6 nm. Yang et al. also reported columnar grain growth in the cross sectional TEM image of FePt-SiO$_2$ films, but the plan-view TEM image showed the grains were interconnected in the planar direction [58]. Various other systems were investigated, but when columnar structure is observed in cross sectional TEM image, in most of the cases the grains are interconnected in the planar direction [59,60]. **Fig. 7** shows typical granular microstructure observed in the FePt-TiO$_x$ system [60]. The FePt grains are interconnected in the planar direction while uniform columnar structure with a smooth surface is obtained in the cross sectional view. However, the film showed soft magnetic properties because of the suppression of the L1$_0$ ordering due to the dissolution of Ti into FePt grains. This means that the driving force for the phase separation between FePt and TiO$_x$ as well as SiO$_2$ is too small to obtain well-isolated grains. From this stand point, Varaprasad et al. have grown FePt-(C,SiO$_2$) and FePt-(C,TiO$_x$) granular films and confirmed certain effect of the usage of mixtures of C and metal oxides for the columnar growth of FePt grains, although the microstructure optimization has not been fully achieved [60]. They also proposed double layer glass/a-NiTa/MgO/FePt-C/FePt-X media, where thin FePt-C (t<6 nm) was used as a template for the second FePt-X (X=SiO$_2$ and TiO$_x$). The initial FePt-C film form well separated granular structure. However, the second untextured layer is formed for t>6 nm. So the system with a lower driving force of phase separation, like FePt-SiO$_2$ and FePt-TiO$_2$, was used as the second layer to suppress the phase separation during the growth in thickness. This approach also showed some promising result.

Shiroyama et al. carried out more comprehensive work on search of metal oxide segregant, i.e., FePt-M$_x$O$_y$ granular films, where M=Cr, Ti, Zr, Nb, W, Al, and Cr [61,62]. **Fig. 8** shows the change of perpendicular H$_c$ as functions of the volume fraction of M$_x$O$_y$. Except for C, all oxides segregant causes the reduction of H$_c$ with the volume fraction of M$_x$O$_y$. This is because Zr, Nb, W, Al, and Ti are all dissolved in FePt, which reduces the driving force for the L1$_0$ ordering. Compared to these, the degree of the degradation of H_c as function of the volume fraction is low for Cr$_2$O$_3$. This is because Cr has large positive enthalpy of mixing with Fe and is not dissolved in FePt. From this figure, one can understand C is a really unique segregant, i.e., it does not lead to the degradation of H_c up to the volume fraction of 40%. **Fig. 9** shows the in-plane and cross-sectional TEM bright field image of FePt–40vol.%Cr$_2$O$_3$ film deposited on a glass substrate with a MgO seed layer [62]. The nominal thickness is 10 nm and all grains are columnarly grown with excellent planar separation. Unfortunately, PMA is not as good as those for FePt-C on MgO seed layer and the coercivity is only 10 kOe with a large in-plane component. The average grain size is 4.8 nm, very fine as compared to FePt-C. However, the size distribution is about 33%, which is too large for a recording medium. Recent investigations on FePt-ZnO$_2$ [63], FePt/AlN [64], FePt-B-Ag [65] all suggest that no systems can match the FePt-C system in view of the planar isolation, narrow size distribution, and high coercivity. Thereafter, research has been focused on how to optimize the granular microstructure in the FePt-C system.

1.3 Optimization of nanostructure of the FePt-C system

The remaining issues for the FePt-C system are summarized as follows;
1) how to grow $L1_0$-FePt grains columnarly in the perpendicular direction to the film without the formation of the second ferromagnetic layer,
2) how to reduce the average grain size to achieve the pitch distance of 7 nm or less while keeping the grain size distribution of less than 15%,
3) how to remove the in-plane component of magnetization.

1.3.1 Columnar Grain Growth

To grow the FePt grains columnarly for the thickness larger than 6 nm, the suppression of the phase separation between FePt and C in the perpendicular direction to the film plane is necessary. When the thickness of FePt ferromagnetic layer becomes thicker than 6 nm, carbon appears to segregate on the surface of FePt grains by the phase separation to the growth direction, which triggers the formation of the second FePt layer. This problem appears to be overcome by modifying the composition of segregant and the sputtering conditions from the fact that the aspect ratios exceeding 1.5 were reported in recent unpublished reports from industrial laboratories [66,67]. However, no details on the materials and processing conditions for achieving the columnar grain structure have been revealed. Therefore, there is a need of getting better understandings on the condition of the columnar growth of the FePt grains.

Although the process is totally different from the industrial one, Varaprasad *et al*. reported a way to achieve the columnar growth of FePt grains by using a concentration graded co-sputtering method [68]. **Fig. 10** shows the plan-view and the cross-sectional TEM images of the FePt-30vol.%C films deposited on MgO (001) single crystals by the standard co-sputtering method (a) (b) and the compositionally graded process (c) (d) [68]. The compositionally graded process means that the films were grown with a sequence of FePt-25vol%C(2)/FePt-30vol%C(2)/FePt-35vol.%C(2)/FePt-25vol%C(2)/FePt-30vol%C(2), where the numbers in the parenthesis is the thickness of each layer in nm. The total thickness of these films is 10 nm, 1.7 times thicker than the critical thickness of the single layer grown by co-sputtering (Fig. 3). In the cross sectional TEM image of the co-sputtered sample, **Fig. 10 (b)**, the film shows the second layer with randomly oriented FePt grains. The plan-view TEM image shows FePt grains are overlapped with other grains and are interconnected, resulting in the large average grain size of 12 nm. Because of this second layer formation, PMA of the film is very poor as shown in **Fig. 10 (a)**. On the other hand, the film fabricated by the compositionally graded process shows a uniform microstructure with the average grain size of 7.8 nm and the aspect ratio of 1.5. The co-sputtered film has small perpendicular H_c and large in-plane hysteresis due to the relatively large grain size and second layer grains. On the other hand, the film grown with the compositionally graded process shows large perpendicular H_c of 3.9 T without in-plane hysteresis. This suggests that controlling the supply of excess amount of carbon after the nucleation of a high number density of FePt grains is effective to suppress the formation of the second ferromagnetic layer and to grow the grains columnarly.

1.3.2 Reduction of in-plane magnetic component

SFD has a close correlation with the signal to noise ratio (SNR) of magnetic recording, and the SFD is influenced by the distributions of size, σ_D, distribution of the anisotropy field of individual grains because of some heterogeneities in chemical composition and the degree of order, and the easy axis distribution. Pisana *et al*. concluded that the H_k distribution is the major

reason for the SFD and its grain size dependence, and the angular distribution of the c-axis of FePt grains is the secondary reason [69]. They also point out that the in-plane and randomly oriented grains and the grain size distribution do not make much contribution to the SFD. On the other hand, Acharya reported that SNR and jitter noise receive significant influence from the in-plane component of magnetization when the grain size of FePt becomes smaller than 7 nm [66]. In the prototype HAMR media, MgO seed layer is used to induce strong [001] texture in the FePt-C magnetic layer [69,70]. However, all FePt-C granular media grown on MgO seed layers contain substantial in-plane components and the origin of the misaligned grains have been a subject of recent TEM studies [71,72,73].

In order to clarify the influence of grain boundary and textures of MgO seed layer, Wang *et al*. investigated the easy axis distribution in FePt-C media deposited on two kinds of MgO [73], i.e., one is single crystalline substrate and the other is a polycrystalline MgO (poly-MgO) underlayer deposited on glass substrates through an *a*-NiTa buffer layer. **Figure 11** shows in-plane and cross-sectional TEM images and their magnetization curves of the FePt-C film deposited on (a) MgO single crystal substrate and (b) polycrystalline MgO seed layer [73]. Both of the films show similar microstructure with the average grain size of about 10 nm and the grain distribution of 1.4 nm. The nominal thickness of the FePt-C layer is 10 nm. Although the films grown on polycrystalline MgO show strong PMA and H_c as seen from the magnetization curves in **Fig. 11,** the squareness and the gradient of the demagnetization curve of the film deposited on the MgO single crystal substrate is far better than that on the poly-MgO seed layer. This indicates that either the angular distribution of the MgO grains or the presence of grain boundaries in the polycrystalline seed layer causes in-plane component of the magnetization in the FePt-C layer. **Fig. 12** shows the orientation maps of the FePt-C granular films grown on (a) MgO(001) single-crystal and (b) poly-MgO underlayer obtained from the plane-view specimens together with the easy axis distribution. The out-of-plane orientation map for the film grown on the single crystalline MgO(001) substrate (Fig.12a) demonstrate almost homogeneous red index color, indicating a prefect [001] texture of FePt grains along the film normal direction. It confirms the good epitaxial growth of FePt nanograins on the MgO(001) single crystal substrate without any misoriented grains. On the other hand, the FePt-C film grown on the poly- MgO underlayer (Fig.12b) shows a distinctly different orientation map. While the majority of the grains are oriented to the [001] direction, variants such as [110] and even [100] (90° misorientation) poles were also detected. The easy axis distribution histograms also show the majority of the misoriented grains have either 48-52° or 90° misorientation. It is known that several FePt grains are nucleated on a MgO grain in the seed layer [73], so the easy axis distribution within the seed layer grain should be very low. This suggests that if the misalignment of [001] texture in the MgO seed layer is improved, the easy axis distribution will be substantially improved. However, even if MgO(001) single crystalline substrate is used, the strong texture does not always develop, suggesting misaligned particles may be nucleating from atomic steps on the MgO (001) surface [74]. Based on high resolution TEM observation, Wicht *et al*. [75] reported that the misalignment of the MgO crystal is smaller than that of the FePt grains. Their work suggests highly textured FePt grains do not develop even if the angular distribution of MgO is small. They conclude that the FePt and MgO are slightly misaligned from the perfect cube-to-cube orientation relationship because of the nucleation of FePt from step edges of MgO seed layer. As the misfit between MgO and FePt on the (001) plane is large, some of faceted planes in FePt show epitaxy with the step edge of MgO, which causes misalignment of FePt on the [001] textured MgO seed layer. On the other hand, Ho *et al*. [72] reported the FePt grains crossing the grain boundaries of MgO underlayer cause the formation of the $L1_0$ lattice with 90° misalignment. These recent investigations suggest the controlled surface roughness, grain size, and texture of the MgO seed

layer are essential to reduce the easy axis distribution of FePt-C media. In addition, search of an alternative seed layer is also important. Some of the promising seed layers are $(Mg_{1-x}Ti_x)O$ [35] and TiN, both of which can be grown with DC sputtering.

1.4 Concluding Remarks

Recent progresses made on the development of FePt based granular films for HAMR media have been reviewed. After many investigations of various FePt-X systems, only the FePt-C and (FePt)Ag-C system remain as promising candidates that can fulfill the requirements for 2 Tbit/in^2 HAMR media. However, there are still several issues to be overcome: reduction of grain size, columnar growth of grains, and reduction of easy axis distribution. To resolve these issues, fundamental studies on the growth mechanisms of the FePt-C ferromagnetic layers on various seed layers is necessary. Some approaches to these issues are addressed in this review. Recent industrial demonstrations of HAMR recording over 1 Tbit/in^2 and its improving endurance test result are encouraging, and the commercial implementation of HAMR appears to be right around the corner. However, further improvement of the microstructure to optimize the read and write properties as well as heat control is essential for achieving higher areal density beyond 2 Tbit/in^2 in the future.

Acknowledgment

1. Shiroishi Y., Fukuda K., Tagawa I., Iwasaki H., Takenoiri S., Tanaka H., Mutoh H. and N. Yoshikawa N. (2009). *IEEE Trans. Magn.*, 2009, **45**, pp. 3816.
2. Klemmer K., Hoydick D., Okumura H., Zhang B. and W. A. Soffa W. A. (1995). *Scripta Metal. Mate.* **33**, pp. 1793.
3. Weller D. and Moser A. (1999). *IEEE Trans. Magn.* **35**, pp. 4423.
4. Rottmayer R. E., Batra S., Buechel D., Challener W. A., Hohlfeld J., Kubota Y., Lu B., Michalcea C., Mountfield K., Pelhos K., Peng C., Rausch T., Seigler M. A., Weller D. and Yang X. M. (2006). *IEEE Trans. Magn.* **42**, pp. 2417.
5. Guarisco D., and Nguy H. (2003). *J Appl Phys.* **93**, pp. 6745.
6. Kryder M. H., Gage E. C., McDaniel T. W., Challener W. A., Rottmayer R. E., Ju G., Hsia Y. T. and Erden M. F. (2008). *Proceedings of the IEEE,* **96**, pp. 1810
7. Stipe B. C., Strand T. C., Poon C. C., Balamane H., Boone T. D., Katine J. A., Li J. L., Rawat V., Nemoto H., Hirotsune A., Hellwig O., Ruiz R., Dobisz E., Kercher D. S., Robertson N., Albrecht T. R. and Terris B. D. (2010). *Nature Photon.* **4**, pp. 484.
8. Varaprasad B. S. D. Ch. S., Takahashi Y. K. and Hono K. (2013). Microstructure Control of L1$_0$-Ordered FePt Granular Film for Heat-Assisted Magnetic Recording (HAMR) Media, JOM, **65**, pp. 853 – 861.
9. Weller D., Parker G., Mosendz O, Champion E, Stipe B, Wang X, Klemmer T, Ju G, and Ajan A, (2014). IEEE Trans. Magn. **50**, pp. 3100108.
10. Wu, A.Q., Kubota Y., Klemmer T, Rausch T, Peng C, Peng Y., Karns D., Zhu X, Yinfeng Ding , Chang E. K. C., Zhao Y., Zhou H., Gao K., Thiele J-H., Seigler M., Ju G., and Edward Gage E. (2013), HAMR Areal Density Demonstration of 1+ Tbpsi on Spinstand, *IEEE Trans. Magn.* **49**, pp. 779.
11. Ristau R. A., Barmak K., Lewis L. H., Coffey K. R. and Howard J. K. (1999). On the relationship of high coercivity and L10 ordered phase in CoPt and FePt thin films, J. Appl. Phys. **86**, 4527 – 4533.
12. Visokay M. R. and Sinclair R. (1995), Direct formation of ordered CoPt and FePt compound thin films by sputtering, *Appl. Phys. Lett.* **66**, pp. 1692 – 1694.
13. Maeda T., Kikitsu A., Kai T., Nagase T., Akiyama J. (2002). Reduction of ordering temperature of an FePt-ordered alloy by addition of Cu, *Appl Phys Lett.*, **80**, pp. 2147.
14. Takahashi Y. K., Ohnuma M., Hono K. (2002). *J Magn Magn Mater.*, **246**, pp. 259.

15. Platt C. L., Wierman K. W., Svedberg E. B., Veerdonk R., Howard J. K., Roy A. G., Laughlin D. E. (2002). $L1_0$ ordering and microstructure of FePt thin films with Cu, Ag, and Au additive, *J Appl Phys.*, **92**, pp. 6104.

16. Maret, M., Brombacher C., Matthes P., Makarav D., Boudet N. and Albercht M. (2012). Anomalous x-ray diffraction measurements of long-range order in (001)-textured $L1_0$ FePtCu thin films, *Phys. Rev. B*, **86**, pp. 024204.

17. Takahashi Y. K., Ohnuma M. and Hono K. (2003). Ordering process of sputtered FePt films, *J. Appl. Phys.* **93**, pp. 7580.

18. Takahashi Y. K. and Hono K. (2005). On low temperature ordering of FePt films, *Scripta Mater.* **53**, pp. 403-409.

19. Takahashi Y. K., Ohkubo T., Ohnuma M. and Hono K. (2003). Size effect on the ordering of FePt granular films, *J. Appl. Phys.* **93**, pp. 7166 – 7168.

20. Takahashi Y. K., Koyama T., Ohnuma M., Ohkubo T. and Hono K. (2004). Size dependence of ordering in FePt nanograins, *J. Appl. Phys.* **95**, pp. 2690 – 2696.

21. Miyazaki T., Kitakami O., Okamoto S., Shimada Y., Akase Z., Murakami Y., Shindo D., Takahashi Y. K., Hono K. (2005), Size effect on the ordering of L10 FePt nanograins, *Phys. Rev. B.* **72**, pp. 144419.

22. Watanabe, M. Takanashi, K. Fujimori, H. (1991). Perpendicular magnetic anisotropy and magneto-optial Kerr effect of FePt/Pt multilayer films, *J. Mag. Mag. Mater.* **113**, pp. 110 – 114.

23. Risokay, M. R. and Sinclair R. (1995), Direct formation of ordered CoPt and FePt compound thin films by sputtering, *Appl. Phys. Lett.* **66**, pp. 1692 – 1694.

24. Farrow R. F. C., Weller D., Marks R. F., Toney M. F., Cebollada A. and Harp G. R., (1996). Control of the axis of chemical ordering and magnetic anisotropy in epitaxial FePt films, *J. Appl. Phys.* **79**, pp. 5967 – 5969.

25. Thiele J.-U., Folks L., Toney M. F. and Weller D. (1998). Perpendicular magnetic anisotropy and magnetic domain structure in sputtered epitaxial FePt (001) $L1_0$ films, *J. Appl. Phys.* **84**, pp. 5686 – 5692.

26. Shima T. Takanashi K. Takahashi Y. K. Hono K. (2002). Preparation and magnetic properties of highly coercive FePt films, *Appl. Phys. Lett.* **81**, pp. 1050 – 1052.

27. Takahashi Y. K., Hono K., Shima T., Takanashi K. (2003). Microstructure and magnetic properties of FePt thin films epitaxially grown on MgO (001) substrates, *J. Mag. Mag. Mater.* **267**, pp. 248 – 255.

28. Shima T., Takanashi K., Takahashi Y. K. and Hono K. (2004). Coercivity exceeding 100 kOe in epitaxially grown FePt sputtered films, *Appl. Phys. Lett.* **85**, pp. 2571 – 2573.

29. Hotta A., Ono T., Hatayama M., Tsumura K., Kikuchi N., Okamoto S., Kitakami O., Shimatsu T. (2014). Magnetic anisotropy and order structure of $L1_0$-FePt(001) single-crystal films grown epitaxially on (001) planes of MgO, $SrTiO_3$, and $MgAl_2O_4$ substrates, *J. Appl. Phys.* **115**, pp. 17B712.

30. Ding Y. F., Chen J. S., Liu E., Sun C. J. and Chow G. M. (2005). Effect of lattice mismatch on chemical ordering of epitaxial $L1_0$ FePt films, *J Appl Phys.*, **97**, pp. 10H303.

31. Jeong S., McHenry M. E. and Laughlin D. E., (2001). Growth and Characterization of $L1_0$ FePt and CoPt 001 Textured Polycrystalline Thin Films, *IEEE Trans. Magn.* **37**, pp. 1309.

32. Xu, Y. F., Chen, J. S. and Wang J. P. (2002). In situ ordering of FePt thin films with face-centered-tetragonal (001) texture on Cr100ÀxRux underlayer at low substrate temperature *Appl. Phys. Lett.*, **80**, pp. 3325.

33. Chen, J. S. Lim, B. C. Hu, J. F. Lim Y. K., Liu, B. and Chow. G. M. (2007). High coercivity $L1_0$ FePt films with perpendicular anisotropy deposited on glass substrate at reduced temperature, *Appl. Phys. Lett.* **90**, pp. 042508.

34. Perumal A. Takahashi Y. K. Seki T. O. Hono K. (2008). Particulate structure of L10 ordered ultrathin FePt films for perpendicular recording, *Appl. Phys. Lett.* **92**, pp. 132508.

35. Varaprasad B. S. D. Ch. S., Takahashi Y. K., Ajan A. and Hono K. (2013). Electrically conductive $(Mg_{0.2}Ti_{0.8})O$ underlayer to grow FePt-based perpendicular recording media on glass substrates, *J. Appl. Phys.* **113**, pp. 203907.

36. Watanabe M, Masumoto T, Ping D. H. and Hono K. (2000). Microstructure and magnetic properties of FePt–Al–O granular thin films, *J. Appl. Phys.* **76**, pp. 3971 – 3973.

37. Ping D. H., Ohnuma M., Hono K., Watanabe M., Iwasa T. and Masumoto T. (2001). Microstructures of FePt–Al–O and FePt–Ag nanogranular thin films and their magnetic properties, *J. Appl. Phys.* **90**, pp. 4708 – 4716.

38. Luo C.P. Liou S. H. Gao L. Liu Y. and Sellmyer D. J. (2000). Nanostructured FePt:B_2O_3 thin films with perpendicular magnetic anisotropy, *Appl. Phys. Lett.* **77**, pp. 2225 – 2227.

39. Peng Y, Zhu J. G., and Laughlin D. E. (2006). $L1_0$ FePt–MgO perpendicular thin film deposited by alternating sputtering at elevated temperature, *J. Appl. Phys.* **99**, pp. 08F907.

40. Ko H. S., Perumal A. and Shin S-C., (2003). Fine control of L10 ordering and grain growth kinetics by C doping in FePt films, *Appl. Phys. Lett.* **82**, pp. 2311 – 2313.

41. Perumal A., Ko H. S., and Shin S. C. (2003). Perpendicular thin films of carbon-doped FePt for ultrahigh-density magnetic recording media, *IEEE Trans. Magn.* **89**, pp. 2320 – 2322.

42. Perumal A., Ko H. S. and Shin S. C. (2003). Magnetic properties of carbon-doped FePt nanogranular films, *Appl. Phys. Lett.* **83**, pp. 3326 – 3328.

43. Chen J. S., Ding Y. F., Lim B. C. and Liu E. J. (2006). Nanogranular $L1_0$ FePt:C composite films for perpendicular recording, *IEEE Trans. Magn.* **42**, pp. 2363 – 2365.

44. Chen, J. S. Lim B. C. Hu, J. F. Liu B. Chow G. M. and Ju G. (2007). Low temperature deposited $L1_0$ FePt–C (001) films with high coercivity and small grain size, *Appl. Phys. Lett.* **91**, pp. 132506.

45. Chen J. S., Hu J. F., Lim B. C., Y. K. Lim Y. K., B. Liu B., G. M. Chow G. M. and G. Ju G. (2008). High coercive $L1_0$ FePt–C (001) nanocomopsite films with small grain size for perpendicular recording media, *J. Appl. Phys.* **103**, pp. 07F517.

46. Chen J. S., Lim B. C., Hu J. F., Ding Y. F., Chow G. M. and Ju G. (2008). Microstructural and magnetic properties of L10 FePt–C (0 0 1) textured nanocomposite films grown on different intermediate layers, *J. Phys. D: Appl. Phys.* **41**, pp. 205001.

47. Li, H., Hu H., Ju J. F., Chow G. M. and Chen J. S. (2011). Effects of CrRu–SiOx underlayer with MgO intermediate layer on the microstructure and magnetic properties of FePt–C thin film, *J. Appl. Phys.* **109**, pp. 07A736.

48. Perumal A. Takahashi Y. K. and Hono K. (2008). $L1_0$ FePt-C nanogranular perpendicular anisotropy films with narrow size distribution, *Appl. Phys. Express* **1**, pp. 101301.

49. Perumal, A. Takahashi Y. K. and Hono K. (2009). FePt-C nanogranular films for perpendicular magnetic recording, *J. Appl. Phys.* **105**, pp. 07B732.

50. Platt C. L., Wierman K. W., Svedberg E. B., van de Veerdonk R., Howard J. K., Roy A. G. and D. E. Laughlin D. E. (2002). $L1_0$ ordering and microstructure of FePt thin films with Cu, Ag, and Au additive, *J. Appl. Phys.* **92**, pp. 6104.

51. Zhang L. Takahashi Y. K. Perumal A. and Hono K. (2010). $L1_0$-ordered high coercivity (FePt)Ag–C granular thin films for perpendicular recording, *J. Mag. Mag. Mater.* **322**, pp. 2658 – 2664.

52. Zhang L., Takahashi Y. K., Hono K., Stipe B. C., Juang J. Y. and Grobis M. (2011). FePtAg-C Nanogranular Film as Thermally Assisted Magnetic Recording (TAR) Media, *IEEE Trans. Magn.* **47**, pp. 4062.

53. Zhang, L. Takahashi, Y. K. Hono, K. Stipe, B. C. Juang, J. Y., Grobis, M. (2011). $L1_0$-ordered FePtAg-C granular thin film for thermally assisted magnetic recording media, *J. Appl. Phys.* **109**, pp. 07B703.

54. Varaprasad, B. S. D. C. S., Takahashi YK., Wang J., Ina T., Nakamura T., Ueno W., Nitta K., Uruga T. and Hono K. (2014). Mechanism of coercivity enhancement by Ag addition in FePt-C granular films for heat assisted magnetic recording media, *Appl. Phys. Lett.* **104**, pp. 222403.

55. Mosendz O., Pisana S., Reiner J. W., Stipe B. and Weller D. (2012). Ultra-high coercivity small-grain FePt media for thermally assisted recording, *J. Appl. Phys.* **111**, pp. 07B729.

56. Pisana S., Mosendz O. Parker G. J. Reiner J. W. Santos T. S. McCallum A. T. , Richter H. J. Weller D. (2013). Effects of grain microstructure on magnetic properties in FePtAg-C media for heat assisted magnetic recording, *J. Appl. Phys.* **113**, pp. 043910.

57. Seki T. O., Takahashi Y. K. and Hono K. (2008). Microstructure and magnetic properties of FePt-SiO_2 granular films with Ag addition, *J. Appl. Phys.* **103**, pp. 023910.

58. Yang E. and Laughlin D.E. (2008). $L1_0$ FePt-oxide columnar perpendicular media with high coercivity and small grain size, *J. Appl. Phys.* **104**, pp. 023904.

59. Chen J. S., Lim B. C., Ding Y. F., Hu J. F., Chow G. M. and Ju, G. (2009). Granular $L1_0$ FePt–X (X=C, TiO2, Ta2O5) nanocomposite films with small grain size for high density magnetic recording, *J. Appl. Phys.* **105**, pp. 07B702.

60. Varaprasad B. S. D. Ch. S. , Chen M. , Takahashi Y. K. and Hono K. (2013). $L1_0$-ordered FePt-based perpendicular magnetic recording media for heat-assisted magnetic recording, *IEEE Trans. Magn.* **49**, pp. 718 – 722.

61. Shiroyama, T. Abe, T. Takahashi Y.K. and Hono, K. (2013). Microstructure and Magnetic Properties of FePt-MO Granular Films, *IEEE Trans. Magn.* **49**, pp. 3616.

62. Shiroyama T., Varaprasad B. S. D. C. S., Takahashi Y. K. and Hono K. (2014). Microstructure and magnetic properties of FePt-Cr_2O_3 films, *IEEE Trans Magn.* **50**, pp. 3202404.1.

63. Dong K. F., Li H. H., Peng Y. G. , Ju G., Chow G. M. and Chen J. S. (2014). $L1_0$ FePt-ZrO_2 (001) nanostructured films with high aspect ratio columnar grains, *Appl. Phys. Lett.* **104**, pp. 192404.

64. Feng C., Zhang E., Xu C. C., Li N., Jiang Y., Yu G. H. and Li B. H. (2011). Magnetic properties and microstructure of $L1_0$-FePt/AlN perpendicular nanocomposite films, *J. Appl. Phys.* **110**, pp. 063910.

65. Granz S.D., Barmak K., Kryder M.K. (2012). Granular $L1_0$ FePt-B and FePt-B-Ag (001) thin films for heat assisted magnetic recording, *J. Appl. Phys.* **111**, pp. 07B709.

66. Acharya A. (2014). Challenges and recent developments in heat assisted magnetic recording media, TMRC 2014, Berkley, August 11-13, 2014.

67. Hellwig O., Challenges in developing FePt $L1_0$ granular thin film media for heat assisted magnetic recording (HAMR), Intermag 2015, AA-05, Beijing, May 11-15, 2015.

68. Varaprasad B. S. D. Ch. S., Wang J., Shiroyama T., Takahashi Y. K. and Hono K. (2015) *IEEE Trans Magn.* in press, DOI: 10.1109/TMAG.2015.2435027.

69. Pisana S., Mosendz O., Parker G. J., Reiner J. W., Santos T. S., McCallum A. T., Richter H. J. and Weller D. (2013), Effects of grain microstructure on magnetic properties in FePtAg-C media for heat assisted magnetic recording, *J. Appl. Phys.* **113**, pp. 043910.

70. Weller D., Mosendz O., Gregory G., Pisana S. and Santos T. S. (2013). FePtX–Y media for heat-assisted magnetic recording, *Phys. Stat. Sol.* **A210**, pp. 1245 – 1260.

71. Wicht S., Neu V., Schultz L., Weller D., Mosendz O., Parker G., Pisana S., and Rellinghaus B. (2013). Atomic resolution structure–property relation in highly anisotropic granular FePt-C films with near-Stoner-Wohlfarth behaviour, *J. Appl. Phys.* **114**, pp. 063906.

72. Ho H., Zhu J., Kulovits A., Laughlin D.E. and Zhu J.G. (2014). Quantitative transmission electron microscopy analysis of multi-variant grains in present $L1_0$-FePt based heat assisted magnetic recording media, *J. Appl. Phys.* **116**, pp. 193510.

73. Wang J., Hata S., Takahashi Y.K., Sepehri-Amin H., Varaprasad B.S.D.Ch.S., Shiroyama T., Schrefl T. and Hono K. (2015). Effect of MgO underlayer misorientation on the texture and magnetic property of FePt–C granular film, *Acta Mater.* 91, 41.

74. Varaprasad B. S. D. Ch. S., Wang J., Shiroyama T., Takahashi Y. K. and Hono K. upublished.

75. Wicht S., Neu V., Schultz L., Mehta V., Jain S., Reiner J., Mosendz O., Hellwig O., Weller D. and B. Rellinghaus B. (2015), Modification of the structural and magnetic properties of granular FePt films by seed layer conditioning, *J. Appl. Phys.* **117**, pp. 013907.

Table

Table 1. HAMR media requirements for 2 and 4 Tbit/in^2 released from the Advanced Storage Technology Consortium (ASTC) [9].

Areal Density (Tbit/in^2)	2	4
Grain size, D (nm)	6	4.3
Center to center distance, D_p (nm)	7	5.1
Size distribution, σ (%)	10 – 15	10 – 15
$\mu_0 M_\mathrm{s}$ of FM layer (T)	0.88	1
$\mu_0 M_\mathrm{s}$ of FM grain (T)	1.1	1.26
K_u (MJ/m^3)	3.5	5
$\mu_0 H_\mathrm{k}$ (T)	8	10
$\sigma_\mathrm{Hk}/H_\mathrm{k}$	5 – 10	5 -10
T_c (°C)	480	430
σ_Tc/Tc (%)	2	2
Angular distribution, σ_θ (°)	2	0.8
Media thickness, t (nm)	9	8.2
Grain aspect ratio (h/D)	1.29	1.6
Grains/bit	6.7	6.2
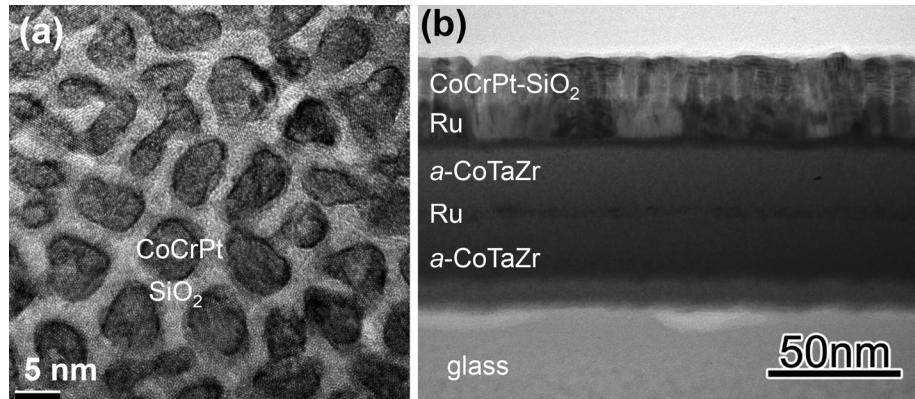
Fig. 1. (a) Plane-view TEM bright field images and (b) the cross sectional TEM image of the currently used perpendicular recording media. CoCrPt ferromagnetic grains of ~8 nm are dispersed in SiO_2 matrix. On the glass substrate, amorphous-CoTaZr soft magnetic underlayer, Ru interlayer that align the [0001] axis of CoCrPt alloy in the perpendicular direction to the film plane are grown.
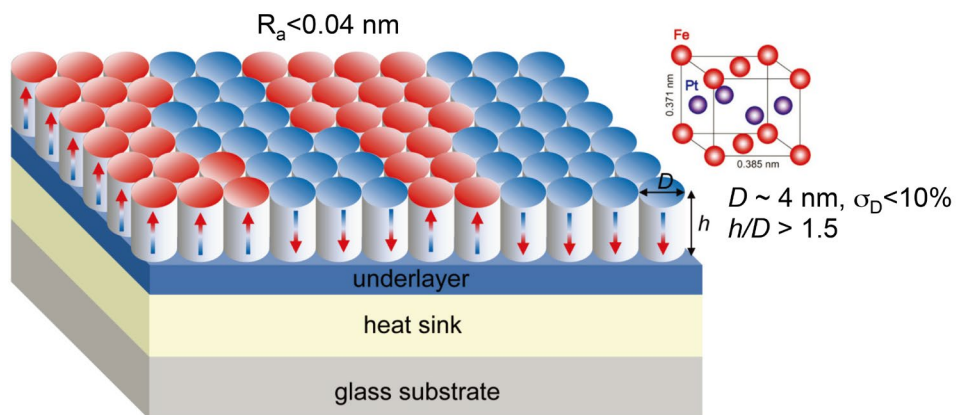
Fig. 2. The ideal structure of a HAMR medium for 4 Tbit/in² arel density. Red and blue colors show the direction of magnetic poles. The $L1_0$-FePt crystal (the upper right figure) must grow columnarly separated by the non-ferromagentic "segregant". The column height to grain diameter ratio h/D must be higher than 1.5 and the diameter of the columnar grains are desired to be less than 4 nm [8].
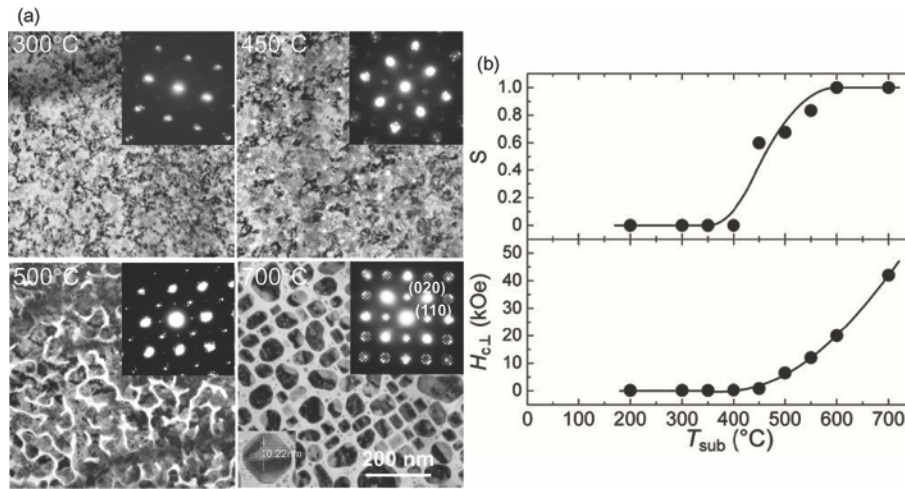
Fig. 3. (a) Plane-view TEM bright field images of FePt films deposited on MgO (001) single crystalline substrates at different temperatures and (b) the degree of $L1_0$ order and coercivity of the films as functions of substrate temperature (T_{sub}) [26].
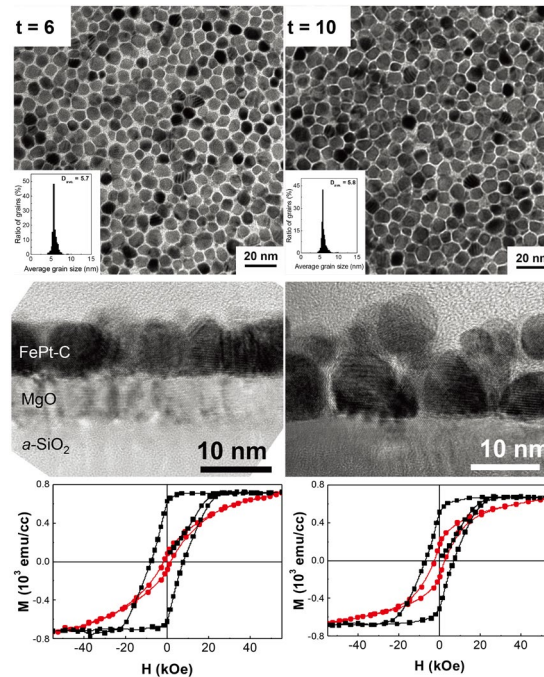
Fig. 4. Plane-view and cross-sectional TEM bright field images and their magnetization curves of FePt-C granular films with nominal thickness, t, of 6 nm and 10 nm. Up to t=6 nm, the film grows with a single layer granular structure, but a second granular layer appears for t>6 nm [48].

17
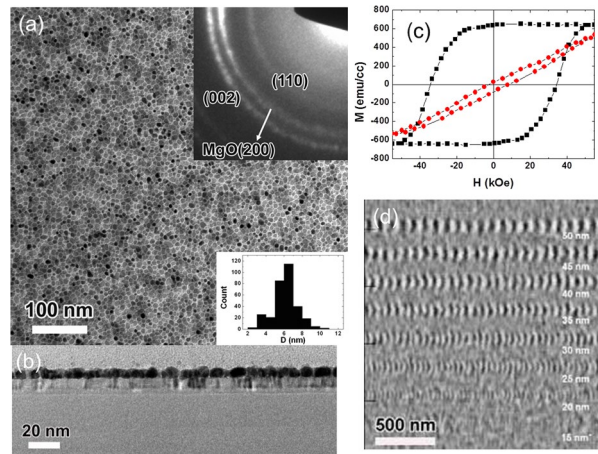
Fig. 5. (a) and (b) Plane-view and cross-sectional TEM bright field images of the $(FePt)_{0.9}Ag_{0.1}$-40vol.%C granular film and (c) magnetization curves, and (d) the patterns of recording bits by the static HAMR head. The mean grain diameter of the FePt grains is 6.1 nm, and their size dispersion is 1.8 nm. Coercivity is 3.7 T, which is five times larger than that of the conventional magnetic recording media. In the recording pattern with the static HAMR head, 15 nm bits were observed with a bit width of 92 nm. Converting to a recording density, this is equivalent to 550 Gbpsi [53].
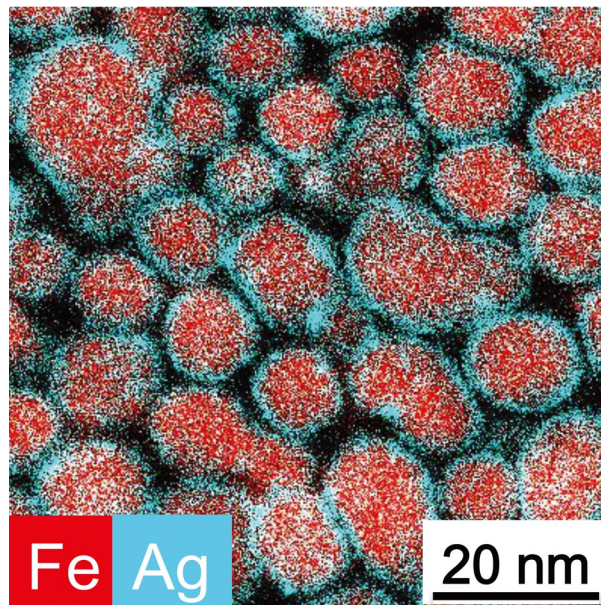

Fig. 6. Scanning transmission electron microscope energy dispersive X-ray spectroscopy (STEM-EDS) elemental maps of Fe and Ag in the $(FePt)_{0.9}Ag_{0.1}$-28vol%C granular film [54].

18
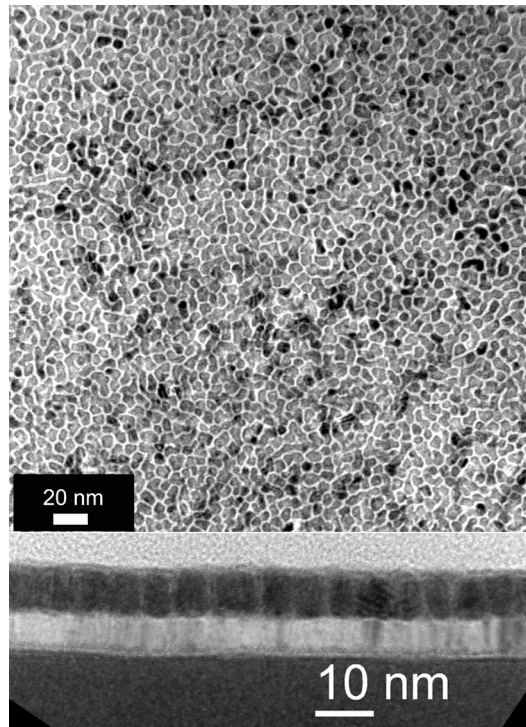
Fig. 7. Plane-view and cross-sectional TEM bright field images of a 8- nm-thick FePt-40vol%TiO$_2$ thin film deposited on a glass substrate through a-NiTa (60 nm)/MgO (10nm) buffer layers. The cross-sectional microstructure shows good columnar structure with aspect ratio of ~2 with less surface roughness whereas plane-view microstructure shows interconnected granular structure [60].
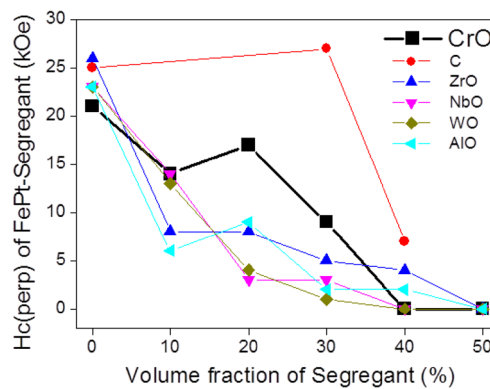

Fig. 8. Change in H_c as a function of the volume fraction of ZrO, NbO, WO, AlO, TiO, Cr$_2$O$_3$ and C [61].
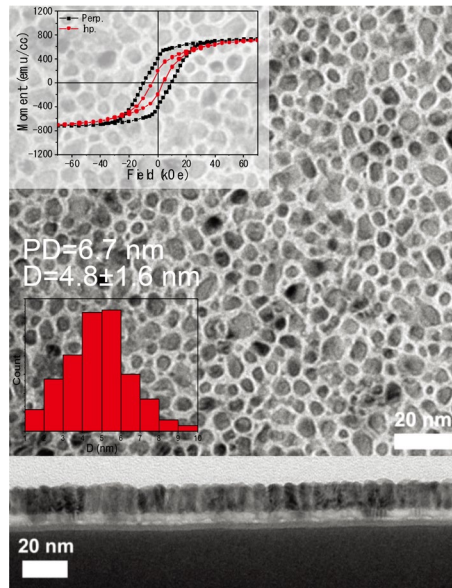
Fig. 9. In-plane and cross-sectional TEM bright field images of the FePt–40vol.%Cr_2O_3 film deposited on a glass substrate with a MgO seed layer [62].
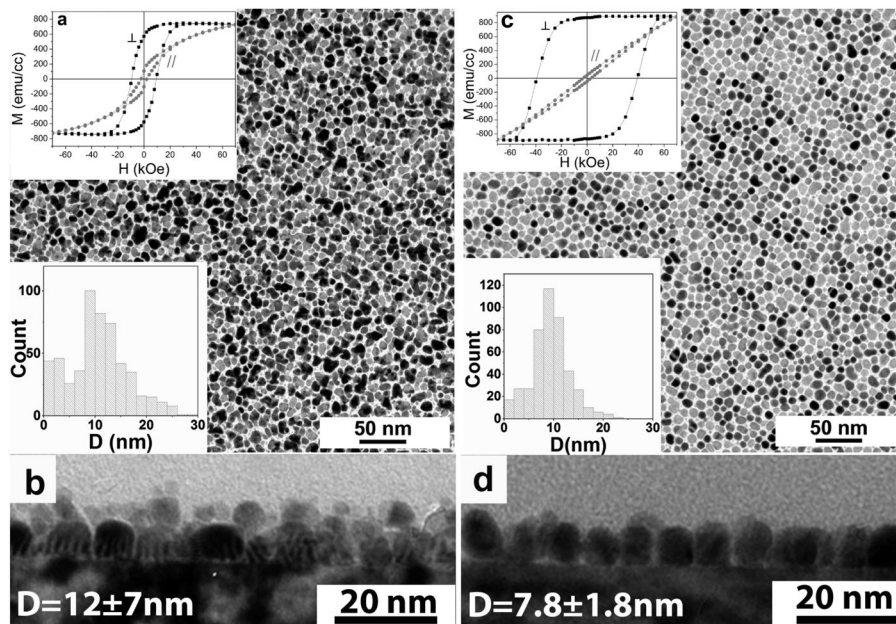

Fig. 10. Plane-view and cross-sectional TEM bright field images of FePt-30vol.%C films deposited by the standard co-sputtering method, (a) and (b), and the compositionally graded process, (c) and (d). The inset figures show their magnetization curves and size distributions of the grains. The compositionally graded process means that the films were grown with a sequence of FePt-25vol%C(2)/FePt-30vol%C(2)/FePt-35vol.%C(2)/FePt-25vol%C(2)/FePt-30vol%C(2), where the numbers in the parenthesis is the thickness of each layer in nm [68].

20
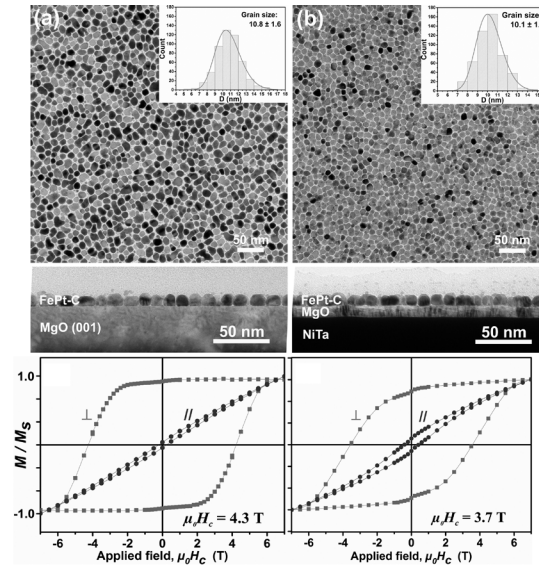
Fig. 11. Plane-view and cross-sectional TEM bright field images of FePt–C granular film on (a) MgO single crystal and (b) polycrystalline MgO underlayer. (Inset: FePt grain size distribution, unit in nm.) The FePt-C magnetic layer was deposited with the concentration graded process of [FePt-48vol.%C (0.25nm)/FePt (0.15nm)]$_{25}$ to obtain the nominal thickness of the FePt-C layer as 10 nm. In-plane and out-of-plane magnetization curves of FePt–C granular film on (a) MgO single crystal and (b) polycrystalline MgO underlayer [73].
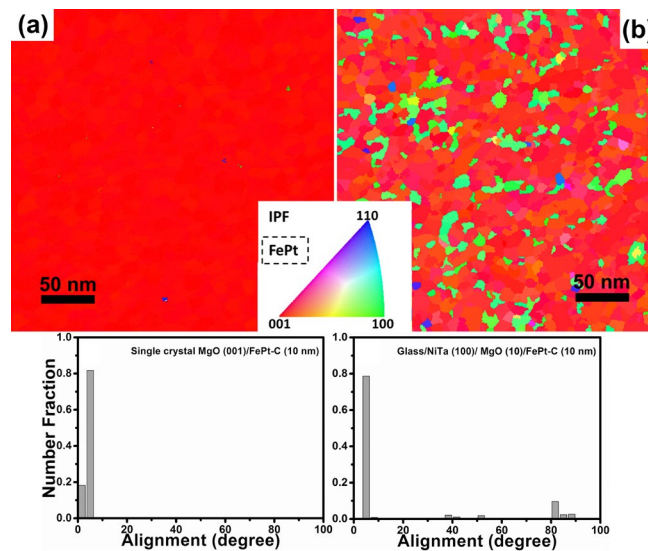
Fig. 12. Orientation maps of FePt–C granular films deposited on (a) a MgO single crystal substrate and (b) a polycrystalline MgO underlayer. The orientation of each grain is given by the reference triangle [73].